Robust Set-Invariance Based Fuzzy Output Tracking Control for Vehicle Autonomous Driving Under Uncertain Lateral Forces and Steering Constraints

Tran Anh-Tu Nguyen, Jagat Jyoti Rath, Thierry-Marie Guerra, Reinaldo Martinez Palhares, Hui Zhang

Robust Set-Invariance Based Fuzzy Output Tracking Control for Vehicle Autonomous Driving Under Uncertain Lateral Forces and Steering Constraints

Article *in* IEEE Transactions on Intelligent Transportation Systems · August 2020

DOI: 10.1109/TITS.2020.3021292

CITATIONS
52

READS
512

5 authors, including:

Anh-Tu Nguyen
Université Polytechnique Hauts-de-France
140 PUBLICATIONS **2,084** CITATIONS
SEE PROFILE

Jagat Jyoti Rath
Institute of Infrastructure Technology Research And Management
50 PUBLICATIONS **1,061** CITATIONS
SEE PROFILE

Thierry-Marie Guerra
Université Polytechnique Hauts-de-France
349 PUBLICATIONS **9,873** CITATIONS
SEE PROFILE

Reinaldo Martínez Palhares
Federal University of Minas Gerais
264 PUBLICATIONS **5,644** CITATIONS
SEE PROFILE

Robust Set-Invariance Based Fuzzy Output Tracking Control for Vehicle Autonomous Driving under Uncertain Lateral Forces and Steering Constraints

Anh-Tu Nguyen*, *Member, IEEE*, Jagat Rath, Thierry-Marie Guerra, Reinaldo Palhares, *Member, IEEE*, Hui Zhang, *Senior Member, IEEE*

***Abstract*—This paper is concerned with a new control method for path tracking of autonomous ground vehicles. We exploit the fuzzy model-based control framework to deal with the time-varying feature of the vehicle speed and the highly uncertain behaviors of the tire-road forces involved in the nonlinear vehicle dynamics. To avoid using costly vehicle sensors for feedback control while favoring the simplest control structure for real-time implementation, a new fuzzy static output feedback (SOF) scheme is proposed. In particular, though the robust set-invariance property and Lyapunov-based arguments, the physical constraints on the steering input saturation and the vehicle state can be taken into account in the control design to improve the driving safety and comfort. The theoretical development relies on the use of fuzzy Lyapunov functions and the non-parallel distributed compensation control concept to reduce the design conservatism. Exploiting some specific convexification techniques, the control design is reformulated as an optimization problem under linear matrix inequalities with a single line search, which are efficiently solved via semidefinite programming techniques. The proposed fuzzy path tracking controller is evaluated through various dynamic driving tests conducted with high-fidelity CarSim/Matlab co-simulations. Moreover, to emphasize the advantages of the new fuzzy SOF controller, a performance comparison with the CarSim driver model is also performed.**

***Index Terms*—Autonomous driving, path tracking, vehicle dynamics, output feedback control, Takagi-Sugeno fuzzy systems, robust set invariance.**

I. Introduction

NOWADAYS, autonomous vehicles have become a reality thanks to significant recent advances in computation and communication technologies. It has been demonstrated that autonomous ground vehicles can improve not only the safety, accessibility and comfort of passengers but also the energy-saving efficiency [1]. For these reasons, driverless vehicle technology has attracted a great deal of attention from academic researchers, industrial companies and local governments [2]. As one of the most important parts of vehicle autonomous navigation, path tracking control of autonomous vehicles has been a significant research topic [2]–[7].

Path tracking control is concerned with designing a steering control law to guide the vehicle to follow a desired trajectory, generated by a vehicle path planner [8], [9]. The key control goal is to achieve path following performance with acceptably small tracking errors and smooth steering actions under various driving conditions [2]. Remarkable contributions on path tracking of autonomous vehicles have been reported in the literature. Generally speaking, the path tracking control strategies can be classified into three main categories [10]: model-free control, vehicle geometric-kinematic-based control and dynamic model-based feedback control. First, model-free controllers, such as PID control [11] or fuzzy logic control [12], [13], [13]–[16], generate the steering actions exclusively based on the tracking errors. Without requiring the vehicle information, these control methods generally require a labor-intensive tuning task to achieve an acceptable path tracking performance [17]. Second, the geometric-kinematic-based path tracking controllers are designed using a vehicle kinematics model [7] and/or geometric relations [3]. Despite their simplicity, these control approaches are only suitable for driving situations, in which the vehicle dynamics can be neglected. Third, the dynamic model-based control design is based on the information of vehicle parameters and dynamics. Here, we focus on these model-based feedback control approaches since they can be used to overcome the above-mentioned drawbacks as indicated in recent comparative studies [2], [17], [18].

Numerous works on path tracking feedback control of autonomous vehicles are available in the open literature, which are mostly based on conventional control theory [3], [17], [19]. Sliding mode control technique was applied to vehicle control in [20], [21]. Despite its robustness with respect to parametric uncertainties and external disturbances, dealing with the chattering issue still leads to both theoretical and practical difficulties [17]. A Lyapunov-based hybrid fault-tolerant controller was proposed in [22] with experimental validations on path tracking of a prototype vehicle. However, the stability and robustness aspects of this control design should be further investigated. An active disturbance rejection controller (ADRC) was developed in [23] for vehicle steering control in the presence of uncertainties and external disturbance. Note that the ADRC requires a fine tuning of several design parameters to ensure a good real-time control performance. Thanks to

This work is supported in part by the French Ministry of Higher Education and Research, in part by the National Center for Scientific Research (CNRS), in part by the Nord-Pas-de-Calais Region under the project ELSAT 2020, in part by the Brazilian agencies CNPq (Grant Number: 307933/2018-0) and FAPEMIG (Grant Number: PPM-00053-17).

A.-T. Nguyen and T.-M. Guerra are with the LAMIH laboratory UMR CNRS 8201, Univ. Polytechnique Hauts-de-France, Valenciennes, France.

J. Rath is with the Department of Informatics, Technische Universitat München, Boltzmannstr. 3, 85748 Garching, Germany.

R. Palhares is with the Department of Electronics Engineering, Federal University of Minas Gerais, Brazil.

H. Zhang is with the School of Transportation Science and Engineering, Beihang University, Beijing, China.

*Corresponding author (email: nguyen.trananhtu@gmail.com).

its intuitive principle and its advantages in dealing with system constraints, model predictive control (MPC) technique has been largely applied to the motion planning [8], [24], [25], path tracking [26] and obstacle avoidance [27], [28] of autonomous vehicles. However, MPC technique requires solving an online optimization problem at each control step, which leads too expensive computational burden for real-time implementation, especially for nonlinear MPC schemes. To avoid this major practical issue while taking into account the forward prediction ability, the preview tracking control has been proposed [10]. However, handling the model uncertainties and the system constraints is still open for this control technique. Takagi-Sugeno (T-S) fuzzy approaches [29] have been proposed to deal with the vehicle tracking control issues [6], [30], [31]. In contrast to model-free fuzzy control [12], [32], [33], rigorous stability analysis and performance proofs can be achieved with T-S fuzzy control approaches [34]. However, fuzzy model-based output feedback control for uncertain systems remains challenging [6], [35].

Despite a significant advance on path tracking of autonomous vehicles, the three following control challenges still require a great deal of research efforts. First, the use of full state feedback design where the effectiveness of the control depends on data acquisition rate is a major constraint [36], [37]. Most of works on the path tracking assume that all the vehicle states can be measured for the real-time control implementation [3], [4]. However, this assumption is generally not realistic in practice. For instance, the sideslip angle and/or the lateral speed, which is crucial for vehicle control, cannot be reliably measured with low-cost sensors [38]–[40]. Therefore, various methods have been proposed to design observers for the estimation of unmeasured vehicle variables, see [36], [41]–[43] and references therein. Then, an observer-based control scheme can be designed for path tracking of autonomous vehicles [6], [30], [40]. Unfortunately, the design of an effective observer-based controller for vehicle path tracking under modeling uncertainties and system constraints still remains open [37]. The second challenge is the reliance of the control design on vehicle modeling. Describing precisely the vehicle nonlinear dynamics is very hard or even impossible [17]. On the other hand, an accurate vehicle model may (unnecessarily) induce many difficulties in the control design. For example, although several semi-empirical models are available to represent accurately the tire-road friction, such as Pacejka magic formula, LuGre model, Burckhardt model [44], these are however hardly exploitable for control purposes due to their strong nonlinearities. Hence, the design of a model-based controller robust to the unmodeled vehicle dynamics, time-varying parameters and external disturbances, is of crucial importance [45]. The third challenge consists in considering the system constraints, *e.g.*, the physical limitations of the steering actuator and the vehicle state constraints, in the control design procedure to improve the driving safety and comfort [22], [46]. This important issue has not been well addressed in the existing literature on the path tracking control [5], [37], especially with output feedback control schemes.

This paper proposes a new fuzzy static output feedback (SOF) controller to *simultaneously* address the three above challenges of vehicle path following. As in [6], fuzzy model-based control is exploited to deal with the nonlinear uncertain vehicle dynamics. Then, the time-varying feature of the vehicle speed and the highly uncertain behaviors of the lateral tire-road forces can be taken into account in the control design to guarantee a satisfactory path tracking performance under different driving conditions. Moreover, our proposed control solution leads to the following new contributions.

- Exploiting the concept of robust invariant set together with Lyapunov-based arguments, the steering input saturation and the vehicle state constraints can be explicitly considered in the control design for safety and confort reasons. Moreover, differently from [38]–[40], here a fuzzy Lyapunov function and a non-parallel distributed compensation (non-PDC) scheme [47] are used to reduce further the design conservatism.
- No additional fuzzy observers as in [6], [30], [37], [40] or dynamic control schemes as in [38], [39] are required to deal with the online unavailability of vehicle state. Then, the proposed fuzzy SOF controller is of much simpler structure than that of these dynamic output feedback control schemes. As a result, the new controller not only improves the reliability of the vehicle control system but also is easier to be implemented in practice.
- The control design procedure is recast as an optimization problem under linear matrix inequalities (LMIs) which can be easily solved with semidefinite programming techniques [48]. Note that the previous robust output feedback control methods in [6] are reformulated as nonconvex problems, inducing numerical difficulties.
- The effectiveness of the proposed fuzzy SOF controller clearly is demonstrated with high-fidelity CarSim/Matlab experiments under dynamic driving conditions.

Notation. For a vector $\mathbf{x}$, $\mathbf{x}_i$ denotes its ith entry. For a square matrix X, $X^\top$ denotes its transpose, $X \succ 0$ means that X is positive definite, $X_{(i)}$ denotes its ith row and $\mathrm{He}\, X = X + X^\top$. $\mathrm{diag}(X_1, X_2)$ denotes a block-diagonal matrix composed of X_1, X_2. I denotes the identity matrix of appropriate dimension. The set of nonnegative integers is denoted by $\mathbb{Z}_+$. For $r \in \mathbb{Z}_+$, we denote $\mathcal{I}_r = \{1, \ldots, r\} \subset \mathbb{Z}_+$. The symbol '$\star$' stands for the terms deduced by symmetry in symmetric block matrices. For convenience, arguments are omitted when their meaning is straightforward.

II. Vehicle Modeling and Problem Formulation

We present hereafter the vehicle modeling for path tracking control, see Fig. 1. The nomenclature is given in Table I.

A. Road-Vehicle Model

A nonlinear single track vehicle model is used to study the vehicle motions, whose dynamics is given as follows [5]:

$$\begin{aligned} M(\dot{v}_x - r v_y) &= F_{xf}\cos\delta - F_{yf}\sin\delta + F_{xr}, \\ M(\dot{v}_y + r v_x) &= F_{xf}\sin\delta + F_{yf}\cos\delta + F_{yr}, \\ I_z \dot{r} &= l_f(F_{xf}\sin\delta + F_{yf}\cos\delta) - l_r F_{yr}. \end{aligned} \tag{1}$$

The front and rear longitudinal forces F_{xi} and lateral forces F_{yi}, for $i \in \{f, r\}$, are caused by the tire-road interaction.

TABLE I
VEHICLE NOMENCLATURE.

Symbol	Description
v_x	longitudinal speed
v_y	lateral speed
β	sideslip angle at the center of gravity (CG)
r	vehicle yaw rate
y_L	lateral deviation error
ψ_L	heading error
δ	steering angle
M	total mass of the vehicle
l_f	distance from CG to the front axle
l_r	distance from CG to the rear axle
l_s	look-ahead distance
η_t	tire length contact
I_z	vehicle yaw moment of inertia
$\mathscr{C}_f$	front cornering stiffness
$\mathscr{C}_r$	rear cornering stiffness

The behaviors of these forces depend on several factors, including slip angles, tire/road characteristics, normal load and so forth [49]. Various nonlinear tire-road friction models such as Pacejka magic formula, Brush model, Burckhardt model, etc., have been developed to represent the tires properties in the extreme handling situations with high lateral acceleration and slip angles [4], [44]. However, the strong nonlinearities involved in these models induce major challenges in the control design. Here, to reduce the design complexity, the following norm-bounded uncertain tire model is used [45]:

$$\begin{aligned} F_{yf} &= 2\mathscr{C}_f\alpha_f = 2\mathscr{C}_f\left(\delta - \frac{v_y + l_f r}{v_x}\right), \\ F_{yr} &= 2\mathscr{C}_r\alpha_r = 2\mathscr{C}_r\frac{l_r r - v_y}{v_x}. \end{aligned} \tag{2}$$

where the cornering stiffness are time-varying to take into account the road friction changes or the nonlinear tire behaviors [6]. These bounded parameters $\mathscr{C}_f \in [\mathscr{C}_{f\min}, \mathscr{C}_{f\max}]$ and $\mathscr{C}_r \in [\mathscr{C}_{r\min}, \mathscr{C}_{r\max}]$, can be represented by

$$\mathscr{C}_f = C_f + \Delta C_f\zeta_f(t), \quad \mathscr{C}_r = C_r + \Delta C_r\zeta_r(t), \tag{3}$$

where $|\zeta_i(t)| \leq 1$, $i \in \{f, r\}$, are *unknown* parameters, and

$$\begin{aligned} C_f &= \frac{\mathscr{C}_{f\max} + \mathscr{C}_{f\min}}{2}, \quad & C_r &= \frac{\mathscr{C}_{r\max} + \mathscr{C}_{r\min}}{2}, \\ \Delta C_f &= \frac{\mathscr{C}_{f\max} - \mathscr{C}_{f\min}}{2}, \quad & \Delta C_r &= \frac{\mathscr{C}_{r\max} - \mathscr{C}_{r\min}}{2}. \end{aligned}$$

For steering control purposes, we consider the small angles assumption and a slow vehicle speed variation. Then, the vehicle lateral dynamics can be derived from (1) and (2) as

$$\begin{bmatrix}\dot\beta \\ \dot r\end{bmatrix} = \begin{bmatrix} -\frac{2(\mathscr{C}_r+\mathscr{C}_f)}{Mv_x} & \frac{2(l_r\mathscr{C}_r - l_f\mathscr{C}_f)}{Mv_x^2} - 1 \\ \frac{2(l_r\mathscr{C}_r - l_f\mathscr{C}_f)}{I_z} & \frac{-2(l_r^2\mathscr{C}_r + l_f^2\mathscr{C}_f)}{I_z v_x} \end{bmatrix}\begin{bmatrix}\beta \\ r\end{bmatrix} + \begin{bmatrix}\frac{2\mathscr{C}_f}{Mv_x} \\ \frac{2l_f\mathscr{C}_f}{I_z}\end{bmatrix}\delta \tag{4}$$

where $v_y = v_x\beta$. The vehicle positioning on the road can be represented by the lateral error y_L from the lane centerline at a lookahead distance l_s, and the heading error ψ_L between the tangent to the road and the vehicle orientation [46]. The dynamics of these error variables are given as follows [4], [5]:

$$\begin{aligned} \dot y_L &= v_x\beta + l_s r + v_x\psi_L, \\ \dot\psi_L &= r - v_x\rho_r, \end{aligned} \tag{5}$$

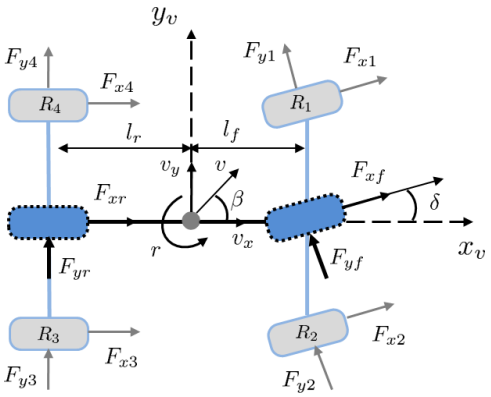

Fig. 1. Vehicle lateral dynamics modeling.

where ρ_r is the road curvature. Note that this amplitude-bounded signal can be obtained from the vehicle vision system.

B. Vehicle Control-Based Model

From the vehicle model (4), the dynamics for path tracking (5), the road-vehicle model can be represented as follows:

$$\dot{\mathbf{x}}(t) = \hat A_v(t)\mathbf{x}(t) + \hat B_v(t)\delta(t) + E_v(t)\mathbf{w}(t), \tag{6}$$

where $\mathbf{x} = \begin{bmatrix}\beta & r & \psi_L & y_L\end{bmatrix}^\top$ is the vehicle state, $\mathbf{w} = \rho_r$ is the system disturbance. The steering control input $\delta(t)$ of the vehicle system (6) is subject to the actuator saturation as

$$\delta(t) = \text{sat}(\mathbf{u}(t)) = \text{sign}(\mathbf{u}(t))\min\left(|\mathbf{u}(t)|, \delta_{\max}\right),$$

where $\mathbf{u}$ is the steering control action to be designed and $\delta_{\max}$ is the physical limitation of the steering angle. The state-space matrices of the control-based model (6) are given by $\hat A_v(t) = A_v(t) + \Delta A_v(t)$, $\hat B_v(t) = B_v(t) + \Delta B_v(t)$ with

$$A_v = \begin{bmatrix} a_{11} & a_{12} & 0 & 0 \\ a_{21} & a_{22} & 0 & 0 \\ 0 & 1 & 0 & 0 \\ v_x & l_s & v_x & 0 \end{bmatrix}, \; B_v = \begin{bmatrix} b_1 \\ b_2 \\ 0 \\ 0 \end{bmatrix}, \; E_v = \begin{bmatrix} 0 \\ 0 \\ -v_x \\ 0 \end{bmatrix},$$

and

$$\begin{aligned} a_{11} &= -\frac{2(C_r + C_f)}{Mv_x}, \quad & a_{12} &= \frac{2(l_rC_r - l_fC_f)}{Mv_x^2} - 1, \\ a_{21} &= \frac{2(l_rC_r - l_fC_f)}{I_z}, \quad & a_{22} &= \frac{-2(l_r^2C_r + l_f^2C_f)}{I_z v_x}, \\ b_1 &= \frac{2C_f}{Mv_x}, & b_2 &= \frac{2l_fC_f}{I_z}. \end{aligned}$$

Moreover, the matrices ΔA_v and ΔB_v represent the system norm-bounded uncertainties caused by the uncertain stiffness. From the expressions of $\mathscr{C}_f$ and $\mathscr{C}_r$ in (3), these uncertain matrices can be represented as

$$\Delta A_v(t) = H_v\Delta(t)L_v, \quad \Delta B_v(t) = H_v\Delta(t)N_v,$$

with

$$H_v = \begin{bmatrix} \frac{2\Delta C_r}{Mv_x} & \frac{2\Delta C_f}{Mv_x} \\ -\frac{2\Delta C_r l_r}{I_z} & \frac{2\Delta C_f l_f}{I_z} \\ 0 & 0 \\ 0 & 0 \end{bmatrix}, \quad L_v = \begin{bmatrix} -1 & -1 \\ \frac{l_r}{v_x} & -\frac{l_f}{v_x} \\ 0 & 0 \\ 0 & 0 \end{bmatrix}^\top,$$

$$\Delta(t) = \text{diag}(\zeta_r(t), \zeta_f(t)), \qquad N_v = \begin{bmatrix}0 & 1\end{bmatrix}^\top.$$

To facilitate the real-time implementation, the path following control design is performed in the discrete-time domain. Then, applying the Euler's discretization

$$\dot{\mathbf{x}}(t) \simeq \frac{\mathbf{x}(\kappa+1)-\mathbf{x}(\kappa)}{T_e}, \quad \forall \kappa \in \mathbb{Z}_+,$$

we can transform system (6) into its discrete-time counterpart

$$\mathbf{x}(\kappa+1) = \hat{A}(v_x)\mathbf{x}(\kappa) + \hat{B}(v_x)\text{sat}(\mathbf{u}(\kappa)) + E(v_x)\mathbf{w}(\kappa) \quad (7)$$

where $\mathbf{z}(\kappa)$ denotes the value of the signal $\mathbf{z}$ at the $\kappa-$instant, and $\Sigma(v_x)$ indicates that matrix Σ explicitly depends on the time-varying speed v_x. The state-space matrices of (7) are given by

$$\begin{aligned} &\hat{A}(v_x) = I + T_e\hat{A}_v(v_x), \quad \hat{B}(v_x) = T_e\hat{B}_v(v_x), \\ &E(v_x) = T_eE_v(v_x), \qquad\qquad T_e = 0.01, \end{aligned}$$

where T_e is the sampling time in second.

Commercial vehicles are usually equipped with an inertial navigation system to measure the yaw rate r and an odometer to measure the vehicle speed v_x. The look-ahead lateral deviation y_L and the heading error ψ_L can be measured by a video camera. The sideslip angle β can be measured by dual antenna GPS systems or Correvit optical sensors. Unfortunately, due to their excessive costs[1], the measurements of β is *unavailable* for real-time implementation in practice [38], [39]. Then, the output equation of the vehicle system (7) is given by

$$\mathbf{y} = \begin{bmatrix} 0 & 1 & 0 & 0 \\ 0 & 0 & 1 & 0 \\ 0 & 0 & 0 & 1 \end{bmatrix} \mathbf{x} = C\mathbf{x}.$$

The controlled output vector $\mathbf{z}$ is defined such that it can represent both the path following performance and the driving comfort. (i) The heading error ψ_L represents both the tracking performance and the future vehicle position error. (ii) The lateral deviation y_L informs about the path following. (iii) The lateral acceleration $a_y \simeq v_x r$ indicates the driving comfort. Then, the controlled output is defined as follows:

$$\mathbf{z} = \begin{bmatrix} \psi_L \\ y_L \\ a_y \end{bmatrix} = \begin{bmatrix} 0 & 0 & 1 & 0 \\ 0 & 0 & 0 & 1 \\ 0 & v_x & 0 & 0 \end{bmatrix} \mathbf{x} = D(v_x)\mathbf{x}. \quad (8)$$

C. Path Following Control Objectives

This paper provides a systematic method to design path following controllers for autonomous vehicles which satisfies the following requirements.

- The control implementation can be done with only low-cost sensors of commercial vehicles. Moreover, the proposed path following controllers must be of simple control structure for real-time application perspective.
- A satisfactory control performance should be achieved under uncertain lateral tire forces and physical constraints on both the vehicle states and the steering input.
- The closed-loop steering control performance is theoretically guaranteed with Lyapunov-based arguments. Furthermore, the control gains can be easily computed with available numerical toolboxes.

[1]For instance, the cost of a Correvit optical sensor used to measure the sideslip angle is about 15k€.

To achieve these challenging control objectives, we propose in the following a new method to design fuzzy SOF controllers in presence of modeling uncertainties and system constraints.

III. Constrained Output Feedback Control Design for Takagi-Sugeno Fuzzy Systems

This section formulates the SOF control problem of fuzzy systems subject to modeling uncertainties and system constraints. Then, the proposed LMI-based control solution is applied to the path following of autonomous ground vehicles.

A. System Description

A class of T-S fuzzy systems subject to modeling uncertainties and actuator saturation with r inference rules can be described as follows [29]:

$$\begin{aligned} &\text{RULE } \mathcal{R}_i: \text{ IF } \xi_1(\kappa) \text{ is } \mathcal{M}_1^i \text{ and} \dots \text{and } \xi_p(\kappa) \text{ is } \mathcal{M}_p^i. \text{ THEN} \\ &\mathbf{x}(\kappa+1) = \hat{A}_i(\kappa)\mathbf{x}(\kappa) + \hat{B}_i(\kappa)\text{sat}(\mathbf{u}(\kappa)) + E_i\mathbf{w}(\kappa), \\ &\quad \mathbf{z}(\kappa) = D_i\mathbf{x}(\kappa), \quad \mathbf{y}(\kappa) = C_i\mathbf{x}(\kappa), \end{aligned} \quad (9)$$

where $\mathbf{x}(\kappa) \in \mathbb{R}^{n_x}$ is the state vector, $\mathbf{u}(\kappa) \in \mathbb{R}^{n_u}$ the control input, $\mathbf{w}(\kappa) \in \mathbb{R}^{n_w}$ the system disturbance, $\mathbf{z}(\kappa) \in \mathbb{R}^{n_z}$ the controlled output, and $\mathbf{y}(\kappa) \in \mathbb{R}^{n_y}$ the measured output, and

$$\hat{A}_i(\kappa) = A_i + \Delta A_i(\kappa), \quad \hat{B}_i(\kappa) = B_i + \Delta B_i(\kappa).$$

The vector of premise variables is defined as $\xi(\kappa) = [\xi_1(\kappa) \cdots \xi_p(\kappa)]^\top \in \mathbb{R}^p$. The ith local state-space matrices with appropriate dimensions $(A_i, B_i, C_i, D_i, E_i)$ are constant.

For the fuzzy system (9), $\mathcal{R}_i$ denotes the ith fuzzy inference rule. $\mathcal{M}_j^i$, with $i \in \mathcal{I}_r$ and $j \in \mathcal{I}_p$, is the fuzzy set. The fuzzy membership functions (MFs) are given by

$$h_i(\xi) = \frac{\prod_{j=1}^p \mu_j^i(\xi_j)}{\sum_{i=1}^r \prod_{j=1}^p \mu_j^i(\xi_j)}, \quad i \in \mathcal{I}_r,$$

where $\mu_j^i(\xi_j)$ represents the grade of membership of ξ_j in the respective fuzzy set $\mathcal{M}_j^i$. Note that the MFs satisfy the following convex sum property:

$$\sum_{i=1}^r h_i(\xi) = 1, \quad 0 \le h_i(\xi) \le 1, \quad \forall i \in \mathcal{I}_r. \quad (10)$$

Let Ω be the set of membership functions satisfying (10), *i.e.*, $h = (h_1(\xi), h_2(\xi), \dots, h_r(\xi)) \in \Omega$. Using the center-of-gravity method for defuzzification, the fuzzy system (9) can be represented in the following compact form [29]:

$$\begin{aligned} \mathbf{x}(\kappa+1) &= \hat{A}(h)\mathbf{x}(\kappa) + \hat{B}(h)\text{sat}(\mathbf{u}(\kappa)) + E(h)\mathbf{w}(\kappa), \\ \mathbf{z}(\kappa) &= D(h)\mathbf{x}(\kappa), \quad \mathbf{y}(\kappa) = C(h)\mathbf{x}(\kappa), \end{aligned} \quad (11)$$

where the uncertain state-space matrices verify the following norm-bounded structures:

$$\begin{aligned} &\hat{A}(h) = A(h) + \Delta A(h), \quad \Delta A(h) = H(h)\Delta(\kappa)L(h), \\ &\hat{B}(h) = B(h) + \Delta B(h), \quad \Delta B(h) = H(h)\Delta(\kappa)N(h), \end{aligned} \quad (12)$$

with

$$\Pi(h) = \sum_{i=1}^{r} h_i(\xi)\Pi_i,\ \Pi \in \{A, B, C, D, E, H, L, N\}. \quad (13)$$

Note that the constant matrices with appropriate dimensions H_i, L_i, N_i, for $\forall i \in \mathcal{I}_r$, defined in (12)-(13), are known, and the time-varying uncertain matrix satisfies $\Delta(\kappa)^\top \Delta(\kappa) \preceq I$. The input saturation function is defined as

$$\text{sat}(\mathbf{u}_l(\kappa)) = \text{sign}(\mathbf{u}_l(\kappa)) \min(|\mathbf{u}_l(\kappa)|, \bar{u}_l), \quad \kappa \in \mathbb{Z}_+,$$

where the control bounds $\bar{u}_l > 0$, for $\forall l \in \mathcal{I}_{n_u}$, are given. The system disturbance $\mathbf{w}$ in (11) is bounded in amplitude and belongs to the following class of function:

$$\mathcal{W}_\phi^\infty = \left\{\mathbf{w} :\ \mathbb{R}^+ \to \mathbb{R}^{n_w}, \quad \mathbf{w}(\kappa)^\top \mathbf{w}(\kappa) \leq \phi,\ \kappa \in \mathbb{Z}_+\right\},$$

with a positive scalar $\phi > 0$.

In many practical situations, the disturbance signal $\mathbf{w}$ can be measured, *e.g.*, the road curvature ρ_r in (6) can be measured by the cameras [10]. Then, incorporating the real-time disturbance information for *feedforward* control may improve the control performance during the transient phases [3]. Hence, we consider the following non-PDC control law [47]:

$$\mathbf{u}(\kappa) = F(h)G(h)^{-1}\mathbf{y}(\kappa) + K(h)\mathbf{w}(\kappa), \quad (14)$$

where the MF-dependent matrices

$$\begin{bmatrix} F(h) & G(h) & K(h) \end{bmatrix} = \sum_{i=1}^{r} h_i(\xi) \begin{bmatrix} F_i & G_i & K_i \end{bmatrix},$$

are to be determined.

Remark 1. If the disturbance $\mathbf{w}$ is not available online, the classical non-PDC control scheme can be directly recovered by setting $K_i = 0$, $\forall i \in \mathcal{I}_r$. Moreover, as can be seen in Theorem 1, the matrix $K(h)$ appears *linearly* in the design conditions. Hence, the incorporation of $K(h)$ into the SOF controller (14) does not induce any additional difficulty when deriving LMI-based design conditions.

Define the dead-zone nonlinearity $\psi(\cdot) : \mathbb{R}^{n_u} \to \mathbb{R}^{n_u}$ as

$$\psi(\mathbf{u}(\kappa)) = \mathbf{u}(\kappa) - \text{sat}(\mathbf{u}(\kappa)).$$

From (11) and (14), the closed-loop fuzzy system can be expressed as follows:

$$\begin{aligned} \mathbf{x}(\kappa+1) &= A_{cl}(h)\mathbf{x}(\kappa) + E_{cl}(h)\mathbf{w}(\kappa) - \hat{B}(h)\psi(\mathbf{u}(\kappa)), \\ \mathbf{z}(\kappa) &= D(h)\mathbf{x}(\kappa), \quad \mathbf{y}(\kappa) = C(h)\mathbf{x}(\kappa), \end{aligned} \quad (15)$$

with

$$\begin{aligned} A_{cl}(h) &= \hat{A}(h) + \hat{B}(h)F(h)G(h)^{-1}C(h), \\ E_{cl}(h) &= E(h) + \hat{B}(h)K(h). \end{aligned}$$

For the control design, we consider the following MF-dependent Lyapunov candidate function:

$$\mathcal{V}(\mathbf{x}, h) = \mathbf{x}^\top \left(\sum_{i=1}^{r} h_i(\xi) Q_i\right)^{-1} \mathbf{x} \triangleq \mathbf{x}^\top Q(h)^{-1}\mathbf{x},$$

with $Q_i \succ 0$, for $\forall i \in \mathcal{I}_r$. The level set associated with $\mathcal{V}(\mathbf{x}, h)$ is defined as

$$\mathscr{L}_\mathcal{V} = \{\mathbf{x} \in \mathbb{R}^{n_x} :\ \mathcal{V}(\mathbf{x}, h) \leq 1,\ \text{for } \forall h \in \Omega\}. \quad (16)$$

The following concept of *robustly invariant set* [50] is crucial to characterize the local stability of the fuzzy system (15).

Definition 1. The set $\mathscr{L}_\mathcal{V}$ defined in (16) is said to be *robustly invariant* with respect to the closed-loop system (15) if there exist two positive scalars α and τ such that

$$\Delta\mathcal{V} + \alpha(\mathcal{V}(\mathbf{x}(\kappa), h(\kappa)) - 1) + \tau(\phi - \mathbf{w}(\kappa)^\top \mathbf{w}(\kappa)) < 0 \quad (17)$$

with

$$\Delta\mathcal{V} = \mathcal{V}(\mathbf{x}(\kappa+1), h(\kappa+1)) - \mathcal{V}(\mathbf{x}(\kappa), h(\kappa)), \quad \forall \kappa \in \mathbb{Z}_+,$$

for $\forall \mathbf{x}(\kappa) \in \mathscr{L}_\mathcal{V} \backslash \{0\}$, $\forall \mathbf{w}(\kappa) \in \mathcal{W}_\phi^\infty$, and $\forall h \in \Omega$. Note that condition (17) guarantees that any closed-loop trajectory of (15) initialized in $\mathscr{L}_\mathcal{V}$ will remain within this set for $\forall \mathbf{w}(\kappa) \in \mathcal{W}_\phi^\infty$ and $\forall \kappa \in \mathbb{Z}_+$. Moreover, if the disturbances vanish, *i.e.*, $\mathbf{w}(\kappa) = 0$, then for $\forall \mathbf{x}(0) \in \mathscr{L}_\mathcal{V}$, the corresponding trajectory converges to the origin with a predefined decay rate α.

This paper proposes an LMI-based solution for the following control problem.

Problem 1. Determine the MF-dependent matrices $F(h)$, $G(h)$ and $K(h)$ of the non-PDC output feedback controller (14) such that system (15) satisfies the following properties.

i) *Property 1:* The set $\mathscr{L}_\mathcal{V}$ defined in (16) is robustly invariant with respect to the fuzzy system (15). Moreover, the controlled output of (15) is $\mathcal{L}_\infty-$norm bounded, *i.e.*, $\mathbf{z}^\top \mathbf{z} \leq \gamma$, for $\gamma > 0$.

ii) *Property 2:* For any $\mathbf{x}(0) \in \mathscr{L}_\mathcal{V}$, the corresponding trajectory of (15) remains inside the polyhedral set of the state space described by

$$\mathscr{S}_x = \left\{\mathbf{x} \in \mathbb{R}^{n_x} : \quad X_{(k)}\mathbf{x} \leq 1, \quad k \in \mathcal{I}_q\right\}, \quad (18)$$

where the given matrix $X \in \mathbb{R}^{q \times n_x}$ characterizes the state constraint domain of system (15).

Remark in Property 1 that minimizing the $\mathcal{L}_\infty-$norm upper bound γ leads to a better control performance.

The following technical lemma is useful to deal with the dead-zone nonlinearity $\psi(\cdot)$.

Lemma 1. [50], [51] Let us consider a MF-dependent matrix $M(h) = \sum_{i=1}^{N} h_i(\xi) M_i \in \mathbb{R}^{n_u \times n_x}$, and the following set:

$$\mathscr{S}_u = \left\{\mathbf{x} \in \mathbb{R}^{n_x} : \left|M(h)Q(h)^{-1}\mathbf{x}\right| \preceq \bar{u}\right\}.$$

If $\mathbf{x} \in \mathscr{S}_u \subset \mathbb{R}^{n_x}$, then

$$\psi(\mathbf{u})^\top S(h)^{-1}\left[\mathbf{u} - \psi(\mathbf{u}) + M(h)Q(h)^{-1}\mathbf{x}\right] \geq 0, \quad (19)$$

for $S(h) = \sum_{i=1}^{N} h_i(\xi) S_i$, and $S_i \in \mathbb{R}^{n_u \times n_u}$, for $\forall i \in \mathcal{I}_r$, are any diagonal positive definite matrices.

B. LMI-Based Non-PDC Output Feedback Control Design

The following theorem provides sufficient conditions to design a SOF controller (14) that can solve Problem 1.

Theorem 1. Consider the fuzzy system (11) with $\mathbf{w} \in \mathcal{W}_\phi^\infty$, and a state constraint domain $\mathscr{S}_x$ defined in (18). If there exist a positive definite MF-dependent matrix $Q(h) \in \mathbb{R}^{n_x \times n_x}$, a diagonal positive definite MF-dependent matrix $S(h) \in$

$\mathbb{R}^{n_u\times n_u}$, MF-dependent matrices $M(h)\in\mathbb{R}^{n_u\times n_x}$, $F(h)\in\mathbb{R}^{n_u\times n_y}$, $G(h)\in\mathbb{R}^{n_y\times n_y}$, $K(h)\in\mathbb{R}^{n_u\times n_w}$, and positive scalars ϵ, γ, α, τ, ρ such that

$$\alpha-\tau\phi>0, \tag{20}$$

$$\begin{bmatrix} Q(h) & \star \\ M(h)_{(l)} & \bar{u}_l^2 \end{bmatrix}\succeq 0,\quad \forall l\in\mathcal{I}_{n_u}, \tag{21}$$

$$\begin{bmatrix} Q(h) & \star \\ X_{(k)}Q(h) & 1 \end{bmatrix}\succeq 0,\quad \forall k\in\mathcal{I}_q, \tag{22}$$

$$\begin{bmatrix} Q(h) & \star \\ D(h)Q(h) & \gamma I \end{bmatrix}\succeq 0, \tag{23}$$

$$\begin{bmatrix} \Upsilon & \star & \star \\ \rho\mathcal{H}(h)^\top & -\rho I & \star \\ \mathcal{L}(h) & 0 & -\rho I \end{bmatrix}\prec 0, \tag{24}$$

for all $h(\xi(\kappa)), h(\xi(\kappa+1))\in\Omega$, where

$$\Upsilon=\begin{bmatrix} (\alpha-1)Q(h) & \star & \star & \star & \star \\ \Upsilon_{21} & -2S(h) & \star & \star & \star \\ 0 & 0 & -\tau I & \star & \star \\ \Upsilon_{41} & \Upsilon_{42} & \Upsilon_{43} & \Upsilon_{44} & \star \\ \Upsilon_{51} & \epsilon F(h)^\top & 0 & \Upsilon_{54} & \Upsilon_{55} \end{bmatrix},$$

$$\mathcal{L}(h)=\begin{bmatrix} L(h)Q(h) & 0 & 0 & 0 & 0 \\ \Theta_1(h)C(h) & \Theta_2(h) & N(h)K(h) & 0 & 0 \\ 0 & 0 & 0 & 0 & \Theta_1(h) \end{bmatrix},$$

$$\mathcal{H}(h)=\begin{bmatrix} 0 & 0 & 0 & H(h)^\top & 0 \\ 0 & 0 & 0 & H(h)^\top & 0 \\ 0 & 0 & 0 & \epsilon H(h)^\top & 0 \end{bmatrix}^\top, \tag{25}$$

and

$$\begin{aligned}
&\Upsilon_{21}=F(h)C(h)+M(h),\quad \Theta_1(h)=N(h)F(h),\\
&\Upsilon_{41}=A(h)Q(h)+B(h)F(h)C(h),\quad \Upsilon_{42}=-B(h)S(h),\\
&\Upsilon_{43}=E(h)+B(h)K(h),\quad \Theta_2(h)=-N(h)S(h),\\
&\Upsilon_{44}=-Q(h_+)=-\sum\nolimits_{i=1}^{N}h_i(\xi(\kappa+1))Q_i,\\
&\Upsilon_{51}=C(h)Q(h)-G(h)C(h),\quad \Upsilon_{54}=\epsilon F(h)^\top B(h)^\top,\\
&\Upsilon_{55}=-\epsilon\left(G(h)+G(h)^\top\right).
\end{aligned}$$

Then, the non-PDC output feedback controller (14) guarantees the two closed-loop properties defined in Problem 1 for the fuzzy system (15).

Proof. Note that inequality (24) implies $G(h)+G(h)^\top\succ 0$. This guarantees that the matrix $G(h)$ is *nonsingular*, thus the validity of the control expression (14).

Applying Schur complement lemma [48], we can prove that (24) is equivalent to

$$\Upsilon+\rho\mathcal{H}(h)\mathcal{H}(h)^\top+\rho^{-1}\mathcal{L}(h)^\top\mathcal{L}(h)\prec 0. \tag{26}$$

Denote $\mathbf{\Delta}(\kappa)=\mathrm{diag}(\Delta(\kappa),\Delta(\kappa),\Delta(\kappa))$. Since $\mathbf{\Delta}^\top\mathbf{\Delta}\preceq I$, using the following matrix fact:

$$\mathbf{X}^\top\mathbf{Y}+\mathbf{Y}^\top\mathbf{X}\preceq\rho\mathbf{X}^\top\mathbf{X}+\rho^{-1}\mathbf{Y}^\top\mathbf{Y},$$

with $\mathbf{X}=\mathcal{H}(h)^\top$ and $\mathbf{Y}=\mathbf{\Delta}\mathcal{L}(h)$, it follows from (26) that

$$\Upsilon+\mathcal{H}(h)\mathbf{\Delta}\mathcal{L}(h)+\mathcal{L}(h)^\top\mathbf{\Delta}^\top\mathcal{H}(h)^\top\prec 0. \tag{27}$$

From the definitions of Υ, $\mathcal{H}(h)$ and $\mathcal{L}(h)$ in (25), inequality (27) can be exactly rewritten in the form

$$\begin{bmatrix} (\alpha-1)Q(h) & \star & \star & \star & \star \\ \Upsilon_{21} & -2S(h) & \star & \star & \star \\ 0 & 0 & -\tau I & \star & \star \\ \hat{\Upsilon}_{41} & \hat{\Upsilon}_{42} & \hat{\Upsilon}_{43} & \Upsilon_{44} & \star \\ \Upsilon_{51} & \epsilon F(h)^\top & 0 & \hat{\Upsilon}_{54} & \Upsilon_{55} \end{bmatrix}\prec 0, \tag{28}$$

where

$$\begin{aligned}
&\hat{\Upsilon}_{41}=\hat{A}(h)Q(h)+\hat{B}(h)F(h)C(h),\quad \hat{\Upsilon}_{42}=-\hat{B}(h)S(h),\\
&\hat{\Upsilon}_{43}=E(h)+\hat{B}(h)K(h),\quad \hat{\Upsilon}_{54}=\epsilon F(h)^\top\hat{B}(h)^\top.
\end{aligned}$$

Multiplying inequality (28) by

$$\begin{bmatrix} I & 0 & 0 & 0 & 0 \\ 0 & I & 0 & 0 & F(h)G(h)^{-1} \\ 0 & 0 & I & 0 & 0 \\ 0 & 0 & 0 & I & \hat{B}(h)F(h)G(h)^{-1} \end{bmatrix},$$

on the left and its transpose on the right leads to

$$\begin{bmatrix} (\alpha-1)Q(h) & \star & \star & \star \\ \mathcal{W}_1(h) & -2S(h) & \star & \star \\ 0 & 0 & -\tau I & \star \\ \mathcal{W}_2(h) & \hat{\Upsilon}_{42} & \hat{\Upsilon}_{43} & \Upsilon_{44} \end{bmatrix}\prec 0, \tag{29}$$

with

$$\begin{aligned}
\mathcal{W}_1(h)&=F(h)G(h)^{-1}C(h)Q(h)+M(h),\\
\mathcal{W}_2(h)&=\hat{A}(h)Q(h)+\hat{B}(h)F(h)G(h)^{-1}C(h)Q(h).
\end{aligned}$$

Pre- and postmultiplying (29) by $\mathrm{diag}(Q(h)^{-1},S(h)^{-1},I,I)$ leads to

$$\begin{bmatrix} (\alpha-1)Q(h)^{-1} & \star & \star & \star \\ \mathcal{W}_3(h) & -2S(h)^{-1} & \star & \star \\ 0 & 0 & -\tau I & \star \\ A_{cl}(h) & -\hat{B}(h) & \hat{\Upsilon}_{43} & \Upsilon_{44} \end{bmatrix}\prec 0, \tag{30}$$

with $\mathcal{W}_3(h)=S(h)^{-1}\left(F(h)G(h)^{-1}C(h)+M(h)Q(h)^{-1}\right)$. Applying Schur complement lemma, we can easily prove that (30) is equivalent to

$$\mathscr{W}^\top Q(h_+)^{-1}\mathscr{W}-\begin{bmatrix} (1-\alpha)Q(h)^{-1} & \star & \star \\ -\mathcal{W}_3 & 2S(h)^{-1} & \star \\ 0 & 0 & \tau I \end{bmatrix}\prec 0, \tag{31}$$

with $\mathscr{W}=\begin{bmatrix} A_{cl}(h) & -\hat{B}(h) & E_{cl}(h)\end{bmatrix}$. Multiplying inequality (31) by $\begin{bmatrix}\mathbf{x}^\top & \psi(\mathbf{u})^\top & \mathbf{w}^\top\end{bmatrix}$ on the left and its transpose on the right, and using the control expression (14) and the closed-loop expression (15), we can obtain

$$\begin{aligned}
&\Delta\mathcal{V}+2\psi(\mathbf{u})^\top S(h)^{-1}\left[\mathbf{u}-\psi(\mathbf{u})+M(h)Q(h)^{-1}\mathbf{x}\right]\\
&\quad+\alpha\mathcal{V}(\mathbf{x})-\tau\mathbf{w}^\top\mathbf{w}<0.
\end{aligned} \tag{32}$$

By Lemma 1, it follows from (32) that

$$\Delta\mathcal{V}+\alpha\mathcal{V}(\mathbf{x})-\tau\mathbf{w}^\top\mathbf{w}<0,\quad \forall\mathbf{x}\in\mathscr{L}_\mathcal{V}\backslash\{0\}. \tag{33}$$

Note that inequality (17) follows directly from (20) and (33). Moreover, pre- and postmultiplying (23) by $\mathrm{diag}(Q(h)^{-1},I)$, then applying Schur complement lemma [48], we obtain

$$D(h)^\top D(h)\preceq\gamma Q(h)^{-1}. \tag{34}$$

It follows directly from (34) that

$$\mathbf{z}^\top \mathbf{z} = \mathbf{x}^\top D(h)^\top D(h)\mathbf{x} \leq \gamma \mathbf{x}^\top Q(h)^{-1}\mathbf{x} \leq \gamma,\ \forall \mathbf{x} \in \mathscr{L}_\mathcal{V},$$

which means that the $\mathcal{L}_\infty-$norm of the controlled output $\mathbf{z}$ is bounded by γ. As a result, Property 1 is proved.

Pre- and postmultiplying (21) by $\mathrm{diag}(Q(h)^{-1}, I)$ yields

$$\begin{bmatrix} Q(h)^{-1} & \star \\ M(h)_{(l)}Q(h)^{-1} & \bar{u}_l^2 \end{bmatrix} \succeq 0, \quad l \in \mathcal{I}_{n_u}. \tag{35}$$

By Schur complement lemma, it is shown that inequality (35) is equivalent to

$$\mathbf{x}^\top Q(h)^{-1}\mathbf{x} \geq \frac{1}{\bar{u}_l^2}\mathbf{x}^\top \mathcal{U}^\top \mathcal{U}\mathbf{x}, \quad \forall \mathbf{x} \in \mathbb{R}^{n_x},\ \forall l \in \mathcal{I}_{n_u}, \tag{36}$$

with $\mathcal{U} = M(h)_{(l)}Q(h)^{-1}$. Since $\mathcal{V}(\mathbf{x}, h) \leq 1$, for $\forall h \in \Omega$, it follows from (36) that $\mathscr{L}_\mathcal{V} \subseteq \mathscr{S}_u$. Hence, if $\mathbf{x} \in \mathscr{L}_\mathcal{V}$, then inequality (19) holds. Following the similar arguments, we can show that (22) guarantees that $\mathscr{L}_\mathcal{V} \subseteq \mathscr{S}_x$. Hence, Property 2 is also proved, thus the proof can be concluded. □

Theorem 1 cannot be directly used for the control design due to the presence of $h(\xi(\kappa)), h(\xi(\kappa+1)) \in \Omega$ in the matrix inequalities (21)-(24). We derive in the following theorem a numerically tractable solution for Problem 1.

Theorem 2. Consider the fuzzy system (11) with $\mathbf{w} \in \mathcal{W}_\phi^\infty$, and a state constraint domain $\mathscr{S}_x$ defined in (18). If there exist positive definite matrices $Q_i \in \mathbb{R}^{n_x \times n_x}$, diagonal positive definite matrices $S_i \in \mathbb{R}^{n_u \times n_u}$, matrices $M_i \in \mathbb{R}^{n_u \times n_x}$, $F_i \in \mathbb{R}^{n_u \times n_y}$, $G_i \in \mathbb{R}^{n_y \times n_y}$, $K_i \in \mathbb{R}^{n_u \times n_w}$, for $i \in \mathcal{I}_r$, and positive scalars ϵ, γ, α, τ, ρ such that the optimization (37) is achievable. Then, the non-PDC static output feedback controller (14) guarantees the closed-loop properties defined in Problem 1 for the fuzzy system (15). Moreover, the $\mathcal{L}_\infty-$norm of the controlled output is minimized.

$$\min_{\nu_i,\ i\in\mathcal{I}_r} \quad \gamma \tag{37}$$
$$\text{s.t. (20), (38), (39), (40) and (41)}$$

where $\nu_i = (\epsilon, \gamma, \alpha, \tau, \rho, Q_i, S_i, M_i, F_i, G_i, K_i)$ and

$$\begin{bmatrix} Q_i & \star \\ M_{i(l)} & \bar{u}_l^2 \end{bmatrix} \succeq 0,\ \forall l \in \mathcal{I}_{n_u},\ \forall i \in \mathcal{I}_r, \tag{38}$$

$$\begin{bmatrix} Q_i & \star \\ X_{(k)}Q_i & 1 \end{bmatrix} \succeq 0,\ \forall k \in \mathcal{I}_q,\ \forall i \in \mathcal{I}_r, \tag{39}$$

$$\begin{bmatrix} Q_j & \star \\ D_i Q_j & \gamma I \end{bmatrix} \succeq 0,\ \forall i \in \mathcal{I}_r,\ \forall j \in \mathcal{I}_r, \tag{40}$$

$$\Psi_{iikq} \prec 0,\ \Psi_{ijkq} + \Psi_{jikq} \prec 0,\ \forall i, j, k, q \in \mathcal{I}_r,\ i < j. \tag{41}$$

The quantity Ψ_{ijkq} in (41) is defined as

$$\Psi_{ijkq} = \begin{bmatrix} \Upsilon_{ijkq} & \star & \star \\ \rho\mathcal{H}_i^\top & -\rho I & \star \\ \mathcal{L}_{ijq} & 0 & -\rho I \end{bmatrix},$$

with

$$\mathcal{H}_i = \begin{bmatrix} 0 & 0 & 0 & H_i^\top & 0 \\ 0 & 0 & 0 & H_i^\top & 0 \\ 0 & 0 & 0 & \epsilon H_i^\top & 0 \end{bmatrix}^\top,$$

$$\mathcal{L}_{ijq} = \begin{bmatrix} L_i Q_j & 0 & 0 & 0 & 0 \\ N_i F_j C_q & -N_i S_j & N_i K_j & 0 & 0 \\ 0 & 0 & 0 & 0 & N_i F_j \end{bmatrix},$$

$$\Upsilon_{ijkq} = \begin{bmatrix} \Gamma_{11} & \star & \star & \star & \star \\ \Gamma_{21} & -2S_j & \star & \star & \star \\ 0 & 0 & -\tau I & \star & \star \\ \Gamma_{41} & -B_i S_j & \Gamma_{43} & -Q_k & \star \\ \Gamma_{51} & \epsilon F_j^\top & 0 & \epsilon F_j^\top B_i^\top & \Gamma_{55} \end{bmatrix},$$

and

$$\begin{aligned} &\Gamma_{11} = (\alpha - 1)Q_j, && \Gamma_{21} = F_j C_q + M_j, \\ &\Gamma_{41} = A_i Q_j + B_i F_j C_q, && \Gamma_{43} = E_i + B_i K_j, \\ &\Gamma_{51} = C_q Q_j - G_j C_q, && \Gamma_{55} = -\epsilon(G_j + G_j^\top). \end{aligned}$$

Proof. Multiplying (38) by $h_i(\xi) \geq 0$ and summing up for $\forall i \in \mathcal{I}_r$, we obtain (21). Similarly, we can prove that (39) implies (22). Moreover, since $h(\xi) = h(\xi(\kappa)) \in \Omega$ and $h(\xi_+) = h(\xi(\kappa+1)) \in \Omega$, it follows from (41) that

$$\begin{aligned} &\sum_{i=1}^r \sum_{k=1}^r \sum_{q=1}^r h_i(\xi)^2 h_k(\xi_+) h_q(\xi) \Psi_{iikq} \\ &+ \sum_{i=1}^r \sum_{i<j}^r \sum_{k=1}^r \sum_{q=1}^r h_i(\xi) h_j(\xi) h_k(\xi_+) h_q(\xi) (\Psi_{ijkq} + \Psi_{jikq}) \\ &= \sum_{i=1}^r \sum_{j=1}^r \sum_{k=1}^r \sum_{q=1}^r h_i(\xi) h_j(\xi) h_k(\xi_+) h_q(\xi) \Psi_{ijkq} \prec 0. \end{aligned} \tag{42}$$

Note that (42) is exactly (24). Hence, inequality (41) implies (24). Similarly, it is shown that (40) implies (23). Then, by the results of Theorem 1, the proof can be concluded. □

Remark 2. The control design procedure in Theorem 2 is expressed as an optimization problem under a set of LMI constraints with a line search over the parameter ϵ. The control feedback gains F_i, G_i and K_i, for $\forall i \in \mathcal{I}_r$, can be easily computed using Matlab software with Yalmip toolbox.

C. Application to Fuzzy-Model-Based Path Tracking Control

1) Vehicle Fuzzy Modeling: Note that the vehicle lateral dynamics (7) and the controlled output $\mathbf{z}$ in (8) depend on the speed terms v_x, $\frac{1}{v_x}$ and $\frac{1}{v_x^2}$, which are measured and bounded

$$v_{\min} \leq v_x \leq v_{\max}, \quad v_{\min} = 5 \text{ [m/s]},\ v_{\max} = 30 \text{ [m/s]}.$$

If v_x, $\frac{1}{v_x}$ and $\frac{1}{v_x^2}$ are *independently* considered as premise variables, then the sector nonlinearity approach [29, Chapter 2] leads to a T-S fuzzy representation with $2^3 = 8$ fuzzy rules[2]. This fuzzy representation would be complex and conservative

[2]Note that the vehicle fuzzy model (13) in [6] is not appropriately represented with four fuzzy rules. Indeed, there are three premise variables therein, *i.e.*, v_x, $\frac{1}{v_x}$ and $\frac{1}{m}$, thus the sector nonlinearity approach should yield an eight-rule vehicle fuzzy model.

for the real-time vehicle control design due to the strong interdependency of these three terms. To overcome this drawback, the following change of premise variable is performed [46]:

$$\frac{1}{v_x} = \frac{1}{v_0} + \frac{1}{v_1}\xi, \tag{43}$$

where the new *time-varying* parameter θ is used to describe the variation of v_x between its lower bound $v_{\min}$ and upper bound $v_{\max}$, with $\xi_{\min} \leq \xi \leq \xi_{\max}$, $\xi_{\min} = -1$, $\xi_{\max} = 1$. Then, using the Taylor's approximation, it follows that

$$v_x \simeq v_0\left(1 - \frac{v_0}{v_1}\xi\right), \quad \frac{1}{v_x^2} \simeq \frac{1}{v_0^2}\left(1 + 2\frac{v_0}{v_1}\xi\right), \tag{44}$$

where

$$v_0 = \frac{2v_{\min}v_{\max}}{v_{\min} + v_{\max}}, \quad v_1 = \frac{2v_{\min}v_{\max}}{v_{\min} - v_{\max}}.$$

Substituting (43) and (44) into (7), we can obtain the following vehicle dynamics:

$$\begin{aligned} \mathbf{x}(\kappa+1) &= \hat{A}(\xi)\mathbf{x}(\kappa) + \hat{B}(\xi)\text{sat}(\mathbf{u}(\kappa)) + E(\xi)\mathbf{w}(\kappa), \\ \mathbf{z}(\kappa) &= D(\xi)\mathbf{x}(\kappa), \quad \mathbf{y}(\kappa) = C\mathbf{x}(\kappa), \end{aligned} \tag{45}$$

which depends *linearly* on the new parameter ξ. Using the sector nonlinearity approach [29], the vehicle model (45) can be *exactly* represented in the following T-S fuzzy form:

$$\begin{aligned} \mathbf{x}(\kappa+1) &= \sum_{i=1}^{2} h_i(\xi)(\hat{A}_i\mathbf{x}(\kappa) + \hat{B}_i\text{sat}(\mathbf{u}(\kappa)) + E_i\mathbf{w}(\kappa)), \\ \mathbf{z}(\kappa) &= \sum_{i=1}^{2} h_i(\xi)D_i\mathbf{x}(\kappa), \quad \mathbf{y}(\kappa) = C\mathbf{x}(\kappa), \end{aligned} \tag{46}$$

where the scalar membership functions are defined as

$$h_1(\xi) = \frac{\xi_{\max} - \xi}{2}, \quad h_2(\xi) = 1 - h_1(\xi).$$

The corresponding state-space matrices are given by

$$\Pi_1 = \Pi(\xi_{\min}), \quad \Pi_2 = \Pi(\xi_{\max}),$$

with $\Pi \in \left\{\hat{A}, \hat{B}, C, D, E\right\}$.

Remark 3. Using the variable change (43) and the Taylor's approximation (44) allows to reduce the number of fuzzy rules from eight to two. This significantly decreases not only the design conservatism but also the numerical complexity for real-time control implementation.

2) Vehicle Design Constraints: First, the steering input must be limited to guarantee not only the driving comfort but also the vehicle closed-loop stability during some specific maneuvers [5]. For the studied autonomous vehicle, the control input limitation $\delta_{\max} = 10$ [deg] is the maximal steering angle. Second, the *trust driving region* should be also taken into account in the control design to improve the safety and comfort [27], [46]. Here, this region can be characterized by the vehicle state constraints as follows.

- The front wheels can be guaranteed to remain inside the road lane with the condition

$$-\frac{(2d-a)}{2} \leq y_L + (l_f - l_s)\,\psi_L \leq \frac{(2d-a)}{2}, \tag{47}$$

where $a = 1.5$ [m] is the vehicle width, and $d = 1.5$ [m] the lane width.

- The following state bounds represent the normal operating conditions of the vehicle:

$$\begin{aligned} |\beta| \leq 0.05 \text{ [rad]}, \quad |r| \leq 0.55 \text{ [rad/s]}, \\ |\psi_L| \leq 0.1 \text{ [rad]}, \quad |y_L| \leq 1 \text{ [m]}. \end{aligned} \tag{48}$$

The state constraints (47) and (48) can be reformulated in the form (18) for the control design.

IV. Illustrative Results and Discussions

This section presents the validation of the proposed fuzzy SOF controller with the high-fidelity CarSim vehicle simulator. To show the practical control performance, we consider dynamic driving scenarios such as race track with variable road curvatures and double lane change (DLC) along with highly variable road friction and speed conditions. The parameters of the CarSim vehicle model considered are $M = 1653$ [kg], $C_f = 95000$ [N/rad], $C_r = 85500$ [N/rad], $l_f = 1.4$ [m], $l_r = 1.646$ [m], and $I_z = 2765$ [kgm^2]. The steer ratio between the driver wheel and the front road steer angle is $R_s = 17.5$. The look-ahead distance to compute the tracking errors is $l_s = 5$ [m]. Note that in CarSim vehicle simulator, based on the sensor information of the driver preview points, the look-ahead distance and lateral error y_L can be easily obtained. To consider the variable friction in the control design, we assume that the parametric uncertainties in the front and rear tire stiffness coefficients are of 15 %, which represents a highly nonlinear behavior of the lateral tire forces.

Solving the LMI-based conditions in Theorem 2 with a decay rate $\alpha = 0.01$, the following control solution is obtained:

$$\begin{aligned} F_1 &= \begin{bmatrix} 0.4219 & -0.1664 & -0.6867 \end{bmatrix}, \\ F_2 &= \begin{bmatrix} -2.8799 & -0.1978 & -0.8417 \end{bmatrix}, \\ G_1 &= \begin{bmatrix} 18.1239 & -0.5172 & -2.5855 \\ -0.0957 & 0.2480 & 0.6858 \\ -0.8100 & 0.6855 & 2.5230 \end{bmatrix}, \\ G_2 &= \begin{bmatrix} 22.8436 & -0.5761 & -2.7658 \\ 0.1206 & 0.2427 & 0.5523 \\ -0.3020 & 0.6578 & 2.0223 \end{bmatrix}, \\ K_1 &= -0.0829, \quad K_2 = -1.5143. \end{aligned}$$

The corresponding Lyapunov matrices are given by

$$Q_1 = \begin{bmatrix} 0.3506 & 0.2718 & -0.0827 & -0.3231 \\ 0.2718 & 31.3393 & -0.7307 & -3.7276 \\ -0.0827 & -0.7307 & 0.2553 & 0.7211 \\ -0.3231 & -3.7276 & 0.7211 & 2.6953 \end{bmatrix},$$

$$Q_2 = \begin{bmatrix} 0.3301 & 0.3164 & -0.0857 & -0.3319 \\ 0.3164 & 26.5060 & -0.6205 & -3.2835 \\ -0.0857 & -0.6205 & 0.2543 & 0.7116 \\ -0.3319 & -3.2835 & 0.7116 & 2.6574 \end{bmatrix},$$

and the minimum $\mathcal{L}_\infty-$gain performance is $\gamma_{\min} = 0.2050$. Remark that the control gains and the Lyapunov matrices obtained for two linear subsystems of the vehicle fuzzy model (46) are clearly different. This represents the advantage of using the proposed nonquadratic Lyapunov function and non-PDC control scheme to handle a large speed variation.

The performance of the proposed fuzzy SOF controller is now evaluated for two dynamic driving scenarios: race course track, and DLC at high speeds. Note that these scenarios are much challenging compared to those considered in [6].

A. Dynamic Driving: Course Track with Variable Curvatures

For the integrated CarSim/Matlab co-simulations, the path tracking on a race course track has been conducted with road curvatures varying in the range $\rho_r \in [-0.02, 0.04]$ and the road friction of $\mu = 0.75$, *i.e.*, $F_{yf} = 2\mu C_f \alpha_f$ and $F_{yr} = 2\mu C_r \alpha_r$. The vehicle traverses the track at dynamic longitudinal speeds in the range $v_x \in [30, 60]$ [km/h]. For regulating the longitudinal speed, the inbuilt PI controller from CarSim has been used. The speed tracking and the path following for the considered driving scenario are shown in Fig. 2. Observe in

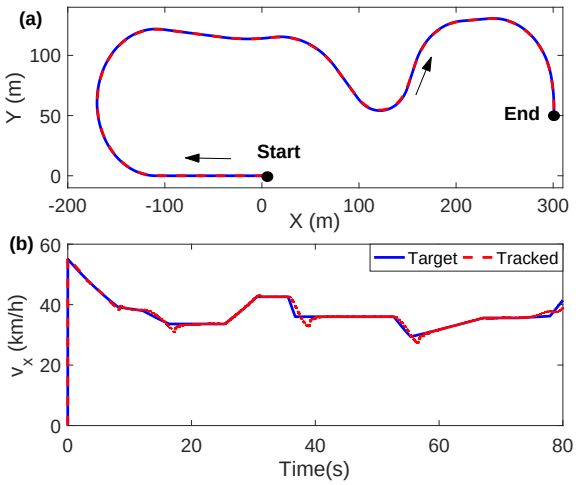

Fig. 2. Tracking performance. (a) Path tracking with the designed fuzzy SOF controller, (b) speed tracking using PI controller from the CarSim simulator.

Fig. 2(a) that even without requiring the online measurement of the sideslip angle, the proposed fuzzy non-PDC controller can guarantee an efficient path following under the presence of nonlinear tire forces and uncertainties. Furthermore, the low speed tracking error as depicted in Fig. 2(b) ensures that safe speed limits across a curve are maintained. The lane deviation errors, *i.e.*, lateral error and heading error, are shown in Fig. 3. Remark that the controlled lane errors are within the constraint limits defined in (48). For comparison analysis, the lane tracking errors with the inbuilt look-ahead preview controller (PC-CSIM) of the CarSim simulator is also illustrated in Fig. 3. Compared to the proposed fuzzy static output feedback (TS-SOF) controller, the lane tracking errors are much larger and cross the lane boundaries, especially at tight curves. Hence, for the considered road friction conditions, the proposed fuzzy SOF controller is able to keep the vehicle on lane which is not the case when using the preview PC-CSIM controller. Subsequently, the illustrations for the vehicle states β, r, the designed steering control input δ and the lateral acceleration are shown in Fig. 4 for both PC-CSIM and fuzzy SOF controllers. It can be seen that the designed control is always within the required constraint of 10 [deg] for both approaches. Further, the sideslip angle does not exceed 0.05

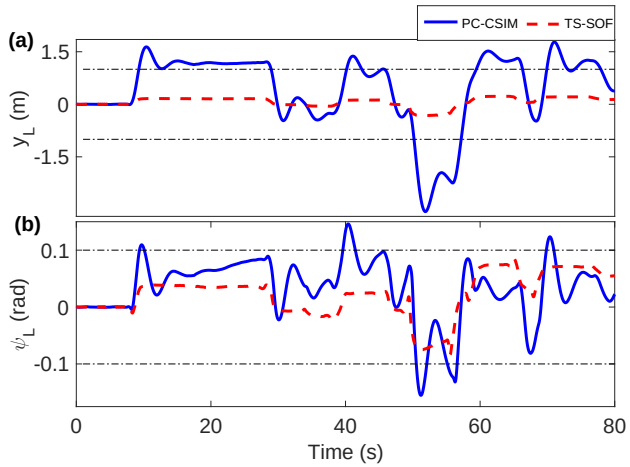

Fig. 3. Path tracking errors. (a) Lateral error y_L, (b) heading error ψ_L.

[rad], which ensures that the tire forces are not saturated. With the maximum yaw rate limited by 0.55 [rad/s], the vehicle maintains a stable control performance. In comparison to the PC-CSIM controller, the proposed non-PDC design provide a smooth steering actions, leading to less oscillatory behaviors and a more stable performance in maintaining the state constraints even when the lateral acceleration is high under the considered friction level.

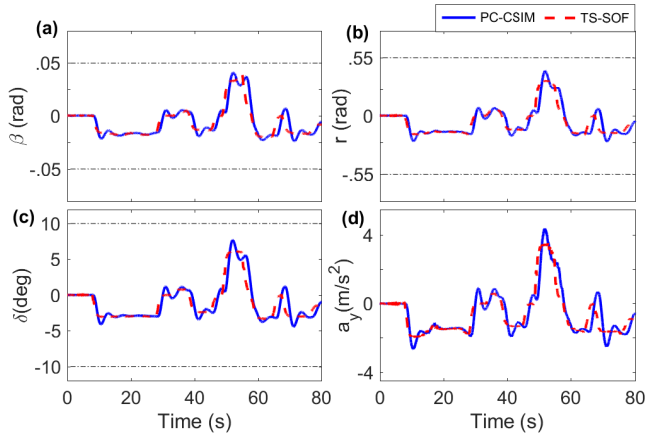

Fig. 4. Vehicle closed-loop behaviors. (a) Sideslip angle β, (b) yaw rate r, (c) designed steering control δ, (d) lateral acceleration a_y.

For further performance analysis, the computed root mean square (RMS) values of the lane tracking error $y_{L_{RMS}}$ [m] and the yaw rate r_{RMS} [rad/s], the maximum values of the sideslip angle $|\beta|_{\max}$ [rad], the lateral acceleration $|a_y|_{\max}$ [m/s^2], and the designed steering input $|\delta|_{\max}$ [deg], are presented in Table II. Note that the proposed TS-SOF controller provides much better path tracking performance for all considered evaluation indexes as shown in Table II. We remark that although the PC-CSIM controller can ensure that the design constraints on the states are maintained, yet the lane errors are quite large indicating a poor tracking performance. However, employing the proposed TS-SOF controller, the vehicle states are constrained and the tracking errors are also small. It should be noted that the maximum value of the controlled

sideslip angle is less than 3 degrees even at a peak lateral acceleration of 4.18 [m/s^2], which indicates that the tire forces are not saturated. Hence, the proposed fuzzy SOF controller can satisfy the path following objectives in the presence of modeling uncertainties with dynamic driving maneuvers.

TABLE II
PATH TRACKING PERFORMANCE COMPARISON FOR $\mu = 0.75$.

Controller	$y_{L_{RMS}}$	r_{RMS}	$\lvert\beta\rvert_{\max}$	$\lvert a_y\rvert_{\max}$	$\lvert\delta\rvert_{\max}$
PC-CSIM	1.125	0.150	0.041	5.17	7.69
TS-SOF	0.155	0.142	0.039	4.18	6.32

B. Extreme Maneuver: DLC at High Speed and Low Friction

To further evaluate the control performance, a dynamic DLC maneuver at high speed of 100 [km/h] has been considered. This maneuver was executed for a road surface with variable friction levels, *i.e.*, $\mu = 1$, $\mu = 0.75$ and $\mu = 0.5$. The corresponding vehicle responses during this maneuver are presented in Fig. 5. We can observe from the responses of the

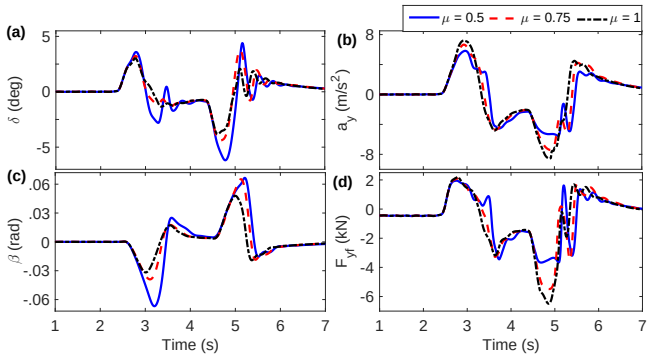

Fig. 5. The designed control for a vehicle executing a DLC under various road friction conditions at 100 km/h. (a) Steering control input, (b) lateral acceleration, (c) sideslip angle, (d) lateral tire force.

steering input and the sideslip angle that with a decrease in friction conditions, the oscillations in the controlled responses increase. For all friction conditions, the maximum steering input does not violate the imposed design constraint. However, when the friction condition decreases too low, the sideslip angle increases and crosses the constraint of 0.05 [rad]. Note that this friction condition with $\mu = 0.5$ is out of the uncertainty range that can be covered by the proposed fuzzy SOF controller. As can be seen from Fig. 5(b), such surface conditions lead to high lateral accelerations greater than 6 [m/s^2], which indicates a very critical operating condition of the vehicle. With the violation of the sideslip constraint, the tire forces approach the saturation region, which may lead to a loss of vehicle stability. To ascertain the performance of the proposed fuzzy SOF controller with low-friction roads, the results obtained for variable speeds in [km/h] are further presented in Table III with $e_{RMS} = y_{L_{RMS}} + (l_f - l_s)\psi_{L_{RMS}}$ [m]. We remark that for all the considered speeds and the friction conditions, the vehicle remains within the lane based on computed values of e_{RMS}. Moreover, due to the extreme DLC at high speeds, the lateral acceleration of the vehicle is very high, *i.e.*, greater than 5 [m/s^2]. However, even for such lateral acceleration levels, the proposed fuzzy SOF design still ensures that all the constraints on the steering input and the vehicle states are satisfied with a satisfactory tracking performance. Such control performance behaviors can be exhibited by the proposed design for other extreme driving conditions such as sudden lane change, driving around extreme curve at high speeds, etc. For illustrations, the results of the controlled driving along a 8-shaped track is depicted in Fig. 6 at a speed of 60 [km/h] with a high surface friction of $\mu = 1$. This track consists of sharp curves and can be visualized as combinations of the S-shaped real-world driving scenario. Note that although the controlled steering and the sideslip angles are constrained within limits, yet a steady-state error on the path tracking is observed. This steady-state error arises as the vehicle navigates a sharp curve at high speed. However, the vehicle remains inside the road lane. In general, such a curve transition with high speeds can introduce oscillations in the designed steering input, which may lead to subsequent saturation. However, using the proposed fuzzy SOF control design, the steering input is smooth without any saturation phenomena. Despite a slight increase of the lane tracking error, the smoothness of the steering control in this case is crucial for comfort reasons.

TABLE III
DLC FOR VARIABLE FRICTION CONDITIONS AT DIFFERENT SPEEDS.

Friction	v_x	e_{RMS}	r_{RMS}	$\lvert\beta\rvert_{\max}$	$\lvert a_y\rvert_{\max}$	$\lvert\delta\rvert_{\max}$
$\mu = 1$	100	0.962	0.132	0.048	7.21	3.81
$\mu = 0.85$	90	0.866	0.124	0.039	6.48	3.67
$\mu = 0.75$	80	0.765	0.116	0.032	5.68	3.58
$\mu = 0.5$	75	0.728	0.114	0.042	5.05	3.86

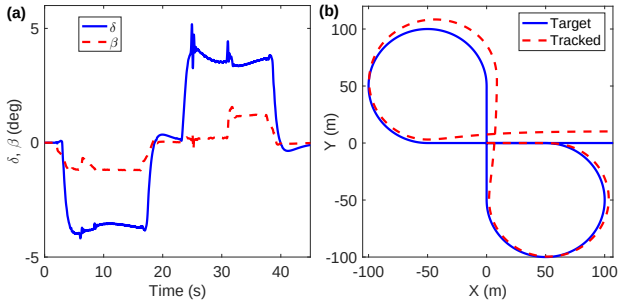

Fig. 6. Path tracking performance obtained with a 8-shaped track with high vehicle speed and surface friction. (a) Sideslip angle and steering input, (b) Path tracking performance.

V. CONCLUDING REMARKS

A new LMI-based control solution for path tracking of autonomous vehicles has been proposed. Using a fuzzy model-based control framework, the vehicle speed variation and the uncertain behaviors of lateral tire forces are effectively handled. In addition, the physical contraints on the steering input and the vehicle state are considered in the control design though the robust set-invariance property and Lyapunov stability arguments. To reduce the design conservatism, fuzzy Lyapunov functions and a non-PDC control scheme are exploited

for theoretical developments. The practical performance of the new SOF path following controller is demonstrated with CarSim/Matlab co-simulations under dynamic driving maneuvers. For future works, we extend the proposed fuzzy SOF scheme to deal with coupled longitudinal-lateral control issues. Experimental validations with real autonomous vehicles under extensive driving conditions will also be considered.

REFERENCES

[1] A. Broggi, P. Medici, P. Zani, A. Coati, and M. Panciroli, "Autonomous vehicles control in the VisLab intercontinental autonomous challenge," *Annu. Rev. Control*, vol. 36, no. 1, pp. 161–171, Apr. 2012.

[2] B. Paden, M. Čáp, S. Z. Yong, D. Yershov, and E. Frazzoli, "A survey of motion planning and control techniques for self-driving urban vehicles," *IEEE Trans. Intell. Veh.*, vol. 1, no. 1, pp. 33–55, Mar. 2016.

[3] J. M. Snider, "Automatic steering methods for autonomous automobile path tracking," Robotics Institute, Carnegie Mellon University, Tech. Rep. CMU-RI-TR-09-08, Feb. 2009.

[4] R. Rajamani, *Vehicle Dynamics and Control*. Boston: Springer, 2012.

[5] A.-T. Nguyen, C. Sentouh, and J.-C. Popieul, "Fuzzy steering control for autonomous vehicles under actuator saturation: Design and experiments," *J. Franklin Inst.*, vol. 355, no. 18, pp. 9374–9395, Dec. 2018.

[6] C. Zhang, J. Hu, J. Qiu, W. Yang, H. Sun, and Q. Chen, "A novel fuzzy observer-based steering control approach for path tracking in autonomous vehicles," *IEEE Trans. Fuzzy Syst.*, vol. 27, no. 2, pp. 278–290, Feb. 2019.

[7] E. Alcala, V. Puig, J. Quevedo, T. Escobet, and R. Comasolivas, "Autonomous vehicle control using a kinematic Lyapunov-based technique with LQR-LMI tuning," *Control Eng. Pract.*, vol. 73, pp. 1–12, 2018.

[8] S. Dixit, U. Montanaro, M. Dianati, D. Oxtoby, T. Mizutani, A. Mouzakitis, and S. Fallah, "Trajectory planning for autonomous high-speed overtaking in structured environments using robust MPC," *IEEE Trans. Intell. Transp. Syst.*, vol. 21, no. 6, pp. 1–14, June 2020.

[9] A. Benloucif, A.-T. Nguyen, C. Sentouh, and J.-C. Popieul, "Cooperative trajectory planning for haptic shared control between driver and automation in highway driving," *IEEE Trans. Indus. Electron.*, vol. 66, no. 12, pp. 9846–9857, Dec. 2019.

[10] S. Xu and H. Peng, "Design, analysis, and experiments of preview path tracking control for autonomous vehicles," *IEEE Trans. Intell. Transp. Syst.*, vol. 21, no. 1, pp. 48–58, Jan. 2020.

[11] P. Zhao, J. Chen, Y. Song, X. Tao, T. Xu, and T. Mei, "Design of a control system for an autonomous vehicle based on adaptive-PID," *Int. J. Adv. Robot. Syst.*, vol. 9, no. 2, p. 44, Jan. 2012.

[12] J. Naranjo, C. Gonzalez, R. Garcia, T. de Pedro, and R. Haber, "Power-steering control architecture for automatic driving," *IEEE Trans. Intell. Transp. Syst.*, vol. 6, no. 4, pp. 406–415, Dec. 2005.

[13] X. Wang, M. Fu, H. Ma, and Y. Yang, "Lateral control of autonomous vehicles based on fuzzy logic," *Control Eng. Pract.*, vol. 34, pp. 1–17, Jan. 2015.

[14] G. Chen and W. Zhang, "Hierarchical coordinated control method for unmanned robot applied to automotive test," *IEEE Trans. Indus. Electron.*, vol. 63, no. 2, pp. 1039–1051, Feb. 2016.

[15] C. Hwang, C. Yang, and J. Y. Hung, "Path tracking of an autonomous ground vehicle with different payloads by hierarchical improved fuzzy dynamic sliding-mode control," *IEEE Trans. Fuzzy Syst.*, vol. 26, no. 2, pp. 899–914, Apr. 2018.

[16] H. Taghavifar and S. Rakheja, "Path-tracking of autonomous vehicles using a novel adaptive robust exponential-like-sliding-mode fuzzy type-2 neural network controller," *Mech. Syst. Signal Process.*, vol. 130, pp. 41–55, Sept. 2019.

[17] N. Amer, H. Zamzuri, K. Hudha, and Z. Kadir, "Modelling and control strategies in path tracking control for autonomous ground vehicles: a review of state of the art and challenges," *J. Intell. Robot. Syst.*, vol. 86, no. 2, pp. 225–254, May 2017.

[18] K. Lee, S. E. Li, and D. Kum, "Synthesis of robust lane keeping systems: Impact of controller and design parameters on system performance," *IEEE Trans. Intell. Transp. Syst.*, pp. 1–13, Oct. 2018.

[19] F. Barbosa, L. Marcos, M. da Silva, M. Terra, and V. Junior, "Robust path-following control for articulated heavy-duty vehicles," *Control Eng. Pract.*, vol. 85, pp. 246–256, Apr. 2019.

[20] G. Tagne, R. Talj, and A. Charara, "Design and comparison of robust nonlinear controllers for the lateral dynamics of intelligent vehicles," *IEEE Trans. Intell. Transp. Syst.*, vol. 17, no. 3, pp. 796–809, 2016.

[21] Y. Jeong, C. Chung, and W. Kim, "Nonlinear hybrid impedance control for steering control of rack-mounted electric power steering in autonomous vehicles," *IEEE Trans. Intell. Transp. Syst.*, pp. 1–10, 2019.

[22] H. Yang, V. Cocquempot, and B. Jiang, "Optimal fault-tolerant path-tracking control for 4WS4WD electric vehicles," *IEEE Trans. Intell. Transp. Syst.*, vol. 11, no. 1, pp. 237–243, Mar. 2010.

[23] Z. Chu, Y. Sun, C. Wu, and N. Sepehri, "Active disturbance rejection control applied to automated steering for lane keeping in autonomous vehicles," *Control Eng. Pract.*, vol. 74, pp. 13–21, May 2018.

[24] J. Suh, H. Chae, and K. Yi, "Stochastic model predictive control for lane change decision of automated driving vehicles," *IEEE Trans. Veh. Technol.*, vol. 67, no. 6, pp. 4771–4782, June 2018.

[25] H. Wang, Y. Huang, A. Khajepour, Y. Zhang, Y. Rasekhipour, and D. Cao, "Crash mitigation in motion planning for autonomous vehicles," *IEEE Trans. Intell. Transp. Syst.*, vol. 20, no. 9, pp. 3313–3323, 2019.

[26] L. Yang, M. Yue, and T. Ma, "Path following predictive control for autonomous vehicles subject to uncertain tire-ground adhesion and varied road curvature," *Int. J. Control, Autom. Syst.*, vol. 17, no. 1, pp. 193–202, 2019.

[27] J. Funke, M. Brown, S. M. Erlien, and J. C. Gerdes, "Collision avoidance and stabilization for autonomous vehicles in emergency scenarios," *IEEE Trans. Control Syst. Technol.*, vol. 25, no. 4, pp. 1204–1216, 2017.

[28] H. Guo, C. Shen, H. Zhang, H. Chen, and R. Jia, "Simultaneous trajectory planning and tracking using an MPC method for cyber-physical systems: A case study of obstacle avoidance for an intelligent vehicle," *IEEE Trans. Indus. Inform.*, vol. 14, no. 9, pp. 4273–4283, Sep. 2018.

[29] K. Tanaka and H. O. Wang, *Fuzzy Control Systems Design and Analysis: A Linear Matrix Inequality Approach*. John Wiley & Sons, 2004.

[30] H. Dahmani, O. Pagès, and A. El Hajjaji, "Observer-based state feedback control for vehicle chassis stability in critical situations," *IEEE Trans. Control Syst. Technol.*, vol. 24, no. 2, pp. 636–643, Mar. 2016.

[31] A.-T. Nguyen, C. Sentouh, H. Zhang, and J.-C. Popieul, "Fuzzy static output feedback control for path following of autonomous vehicles with transient performance improvements," *IEEE Trans. Intell. Transp. Syst.*, vol. 21, no. 7, pp. 3069–3079, July 2020.

[32] B. Boada, M. Boada, and V. Diaz, "Fuzzy-logic applied to yaw moment control for vehicle stability," *Vehicle Syst. Dyn.*, vol. 43, no. 10, pp. 753–770, Feb. 2005.

[33] S. Wu, H. Chiang, J. Perng, C. Chen, B. Wu, and T. Lee, "The heterogeneous systems integration design and implementation for lane keeping on a vehicle," *IEEE Trans. Intell. Transp. Syst.*, vol. 9, no. 2, pp. 246–263, June 2008.

[34] A.-T. Nguyen, T. Taniguchi, L. Eciolaza, V. Campos, R. Palhares, and M. Sugeno, "Fuzzy control systems: Past, present and future," *IEEE Comput. Intell. Mag.*, vol. 14, no. 1, pp. 56–68, Feb. 2019.

[35] A.-T. Nguyen, P. Coutinho, T.-M. Guerra, R. Palhares, and J. Pan, "Constrained output-feedback control for discrete-time fuzzy systems with local nonlinear models subject to state and input constraints," *IEEE Trans. Cybern.*, pp. 1–12, 2020, DOI: 10.1109/TCYB.2020.3009128.

[36] B. Zhang, H. Du, J. Lam, N. Zhang, and W. Li, "A novel observer design for simultaneous estimation of vehicle steering angle and sideslip angle," *IEEE Trans. Indus. Electron.*, vol. 63, no. 7, pp. 4357–4366, July 2016.

[37] C. Hu, Z. Wang, H. Taghavifar, J. Na, Y. Qin, J. Guo, and C. Wei, "MME-EKF-based path-tracking control of autonomous vehicles considering input saturation," *IEEE Trans. Veh. Technol.*, vol. 68, no. 6, pp. 5246–5259, June 2019.

[38] A.-T. Nguyen, C. Sentouh, and J.-C. Popieul, "Sensor reduction for driver-automation shared steering control via an adaptive authority allocation strategy," *IEEE/ASME Trans. Mechatron.*, vol. 23, no. 1, pp. 5–16, Feb. 2018.

[39] J. Wang, M. Dai, G. Yin, and N. Chen, "Output-feedback robust control for vehicle path tracking considering different human drivers' characteristics," *Mechatronics*, vol. 50, pp. 402–412, Apr. 2018.

[40] C. Ting, "An output-feedback fuzzy approach to guaranteed cost control of vehicle lateral motion," *Mechatronics*, vol. 19, pp. 304–312, 2009.

[41] K. Nam, S. Oh, H. Fujimoto, and Y. Hori, "Estimation of sideslip and roll angles of electric vehicles using lateral tire force sensors through RLS and Kalman filter approaches," *IEEE Trans. Indus. Electron.*, vol. 60, no. 3, pp. 988–1000, Mar. 2013.

[42] M. Gadola, D. Chindamo, M. Romano, and F. Padula, "Development and validation of a Kalman filter-based model for vehicle slip angle estimation," *Veh. Syst. Dyn.*, vol. 52, no. 1, pp. 68–84, Dec. 2014.

[43] A.-T. Nguyen, T.-M. Guerra, C. Sentouh, and H. Zhang, "Unknown input observers for simultaneous estimation of vehicle dynamics and driver torque: Theoretical design and hardware experiments," *IEEE/ASME Trans. Mechatron.*, vol. 24, no. 6, pp. 2508–2518, Dec. 2019.

[44] L. Li, F.-Y. Wang, and Q. Zhou, "Integrated longitudinal and lateral tire/road friction modeling and monitoring for vehicle motion control," *IEEE Trans. Intell. Transp. Syst.*, vol. 7, no. 1, pp. 1–19, Mar. 2006.
[45] H. Du, N. Zhang, and G. Dong, "Stabilizing vehicle lateral dynamics with considerations of parameter uncertainties and control saturation through robust yaw control," *IEEE Trans. Veh. Technol.*, vol. 59, no. 5, pp. 2593–2597, June 2010.
[46] A.-T. Nguyen, C. Sentouh, and J.-C. Popieul, "Driver-automation cooperative approach for shared steering control under multiple system constraints: Design and experiments," *IEEE Trans. Ind. Electron.*, vol. 64, no. 5, pp. 3819–3830, May 2017.
[47] A.-T. Nguyen, P. Chevrel, and F. Claveau, "Gain-scheduled static output feedback control for saturated LPV systems with bounded parameter variations," *Automatica*, vol. 89, pp. 420–424, Mar. 2018.
[48] S. Boyd, L. El Ghaoui, E. Feron, and V. Balakrishnan, *Linear Matrix Inequalities in System and Control Theory*. Philadelphia: SIAM, 1994.
[49] J. Kim, "Identification of lateral tyre force dynamics using an extended Kalman filter from experimental road test data," *Control Eng. Pract.*, vol. 17, no. 3, pp. 357–367, Mar. 2009.
[50] S. Tarbouriech, G. Garcia, J. Gomes da Silva Jr., and I. Queinnec, *Stability and Stabilization of Linear Systems with Saturating Actuators*. London: Springer-Verlag, 2011.
[51] A.-T. Nguyen, T. Laurain, R. Palhares, and J. Lauber, "LMI-based control synthesis of constrained T-S systems subject to $\mathscr{L}_2$ or $\mathscr{L}_\infty$ disturbances," *Neurocomputing*, vol. 207, pp. 793–804, Sept. 2016.

Anh-Tu Nguyen (M'18) is an Associate Professor at the Université Polytechnique des Hauts-de-France, Valenciennes, France. He received the degree in engineering and the M.Sc. degree in automatic control from Grenoble Institute of Technology, France, in 2009, and the Ph.D. degree in automatic control from the Université Polytechnique Hauts-de-France, Valenciennes, France, in 2013.

After working a short period in 2010 at the French Institute of Petroleum, Rueil-Malmaison, France, Dr. Nguyen began his doctoral program at the University of Valenciennes, France, in collaboration with the VALEO Group. From February 2014 to August 2018, Dr. Nguyen was a postdoctoral researcher at the laboratory LAMIH UMR CNRS 8201, Valenciennes, France, and the laboratory LS2N UMR CNRS 6004, Nantes, France. Dr. Nguyen's research interests include robust control, constrained control systems, human-machine shared control for intelligent vehicles (see more information at https://sites.google.com/view/anh-tu-nguyen).

Jagat Rath received the B.Tech. degree in electrical engineering from KIIT University, Bhubaneswar, India, in 2010, the M.Tech. degree in mechatronics from Academy of Scientific and Innovative Research, Chennai, India, in 2012, and the Ph.D. degree in embedded systems and control engineering from Kyungpook National University, Daegu, South Korea, in 2016. From 2016-2018, he was a postdoctoral researcher at LAMIH UMR CNRS 8201, Valenciennes, France. From 2019 to 2020, he was a postdoctoral fellow at Technical University of Munich. He has worked on projects related to autonomous driving and human-machine collaborative driving funded by Renault, Ford, Continental among others. His research interests include nonlinear state estimation and control, human-machine interaction management, interval estimation and fault diagnosis/control for mechatronic systems.

Thierry-Marie Guerra is a Full Professor at the Polytechnic University Hauts-de-France, France. He received his Ph.D. degree in automatic control in 1991 and the HDR in 1999. From 2009 to 2019, he was head of the Laboratory of Industrial and Human Automation, Mechanics and Computer Science (LAMIH CNRS UMR 8201) (148 researchers and staff, 110 PhD students and postdocs) http://www.univ-valenciennes.fr/LAMIH/. He is chair of the Technical Committee 3.2 "Computational Intelligence in Control" for IFAC, member of the IFAC TC 7.1 "Automotive Control", Area Editor of the international journals: Fuzzy Sets & Systems and IEEE Transactions on Fuzzy Systems. His topics of interest are wine, hard rock, stamps, nonlinear control, LPV, Takagi-Sugeno models control and observation, nonquadratic Lyapunov functions and applications to mobility, soft robotics and disabled persons.

Reinaldo Palhares (M'14) is currently a Full Professor with the Department of Electronics Engineering, Federal University of Minas Gerais, Belo Horizonte, Brazil. Palhares received his Ph.D. degree in Electrical Engineering from the UNICAMP, Brazil, in 1998. His main research interests include robust control, fault detection, diagnosis and prognosis and artificial intelligence.

Prof. Palhares has been serving as an Associate Editor for the IEEE Transactions on Industrial Electronics and Guest Editor for The Journal of The Franklin Institute – Special Section on "Recent Advances on Control and Diagnosis via Process Measurements", for the IEEE/ASME Transactions on Mechatronics – Focused Section on "Health Monitoring, Management and Control of Complex Mechatronic System", and for the IEEE Transactions on Industrial Electronics – Special Section on "Artificial Intelligence in Industrial Systems" (see more information at http://www.ppgee.ufmg.br/ palhares).

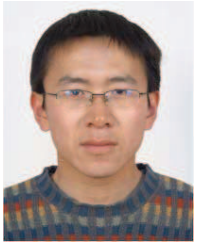

Hui Zhang is a Professor from Beihang University, Beijing, China. He received the BSc. degree in mechanical design manufacturing and automation from the Harbin Institute of Technology, China in 2006, the MSc. degree in automotive engineering from Jilin University, China in 2008, and the Ph.D. degree in mechanical engineering from University of Victoria, Canada in 2012.

Dr. Zhang's research interests include Diesel engine aftertreatment systems, vehicle dynamics and control, mechatronics, networked control systems, and multi-agent systems. He is a coauthor of over 80 peer-reviewed journals. In 2017, he published one book entitled "Modeling, Dynamics, and Control of Electrified Vehicles" with Elsevier Woodhead Publishing.

Dr. Zhang is a recipient of 2017 IEEE Transactions on Fuzzy Systems Outstanding Paper Award and 2018 SAE Ralph R. Teetor Educational Award. He is a member of SAE International, a senior member of IEEE and a member of ASME. Dr. Zhang has served on the IFAC Technical Committee on Automotive Control, ASME Automotive and Transportation Systems Technical Committee. Dr. Zhang serves as an Associate Editor for IEEE Transactions on Vehicular Technology, SAE International Journal of Vehicle Dynamics, Stability, and NVH, SAE International Journal of Connected and Automated Vehicles; Board member of International Journal of Hybrid and Electric Vehicles, Mechanical Systems and Signal Processing; Guest Editor of various international journals; Conference Editorial Board of ASME Dynamic Systems and Control Division, and American Control Conference.